High-spin structure of neutron-rich Se, As, Ge, and Ga isotopes

N. Yoshinaga,[1,*] K. Higashiyama,[2,†] and P. H. Regan[3,‡]
[1]*Department of Physics, Saitama University, Saitama City 338-8570, Japan*
[2]*Department of Physics, Chiba Institute of Technology, Narashino, Chiba 275-0023, Japan*
[3]*Department of Physics, University of Surrey, Guildford GU2 7XH, United Kingdom*
(Received 17 June 2008; published 23 October 2008)

Full-fledged shell-model calculations have been performed for neutron-rich Se, As, Ge, and Ga isotopes using a valence space made up from nucleons occupying the $g_{9/2}$, $p_{1/2}$, $p_{3/2}$, and $f_{5/2}$ orbitals. The calculated energies and electromagnetic transitions are compared with the experimental data which is available on these nuclei. Pair-truncated shell model calculations have also been carried out to investigate the structure of the high-spin states, with particular focus on the effect of the alignment of neutrons in the $g_{9/2}$ orbital.

DOI: 10.1103/PhysRevC.78.044320 PACS number(s): 21.60.Cs, 23.20.Lv, 27.50.+e

I. INTRODUCTION

With the advent of radioactive ion beams, it is now possible to create radioactive nuclei with significant neutron excess. In particular, in light nuclei exciting phenomena have been suggested including phenomena such as neutron skins, haloes, and the emergence of new magic numbers. For heavier systems, new structural phenomena might also be revealed. Recent reports following initial studies with projectile fragmentation [1–3] and deep-inelastic reactions [4–7] have suggested the presence of a possible subshell closure for neutron number $N = 32$ associated with a large single-particle gap between the neutron $p_{3/2}$ and $p_{1/2}$ orbitals. There is ongoing interest into the question of robustness for the traditional magic numbers at $N, Z = 28$, (40), and 50, and how the related suggestion of new subshell closures at nucleon numbers 32 and 34 varies as a function of neutron/proton number [8].

A related issue is how high-spin structure is affected as the neutron number approaches to the magic number $N = 50$. Jones *et al*. recently reported on the structure of near-yrast states in the $N = 46, 48$ isotones ^{80,82}Se populated via heavy-ion deep-inelastic reactions [9]. In that work, a shell model analysis was made assuming three orbitals for neutrons and protons, with the aim of investigating the effect of proton single-particle energies above the $Z = 28$ shell for $N \sim 50$. The states in ^{80,82}Se were interpreted in terms of the alignment of $g_{9/2}$ neutrons and proton excitations from the $f_{5/2}$ subshell to the $p_{3/2}$ or $p_{1/2}$ orbital.

In the current work we present results from fully-shell model calculations for $_{34}$Se, $_{33}$As, $_{32}$Ge, and $_{31}$Ga isotopes assuming a phenomenological pairing plus quadrupole-quadrupole interactions for both even-even and odd-mass nuclei. In our previous paper on selenium isotopes [9] only three valence orbitals were taken for each neutron and proton space. In the current work all configurations with four single-particle orbitals, $g_{9/2}$, $p_{1/2}$, $p_{3/2}$, and $f_{5/2}$, between the magic numbers 28 and 50 are included. We also investigate the neighboring even-even isotopes and odd-mass nuclei allowing the predicted excitation energies and electromagnetic transitions to be compared with experiment over a wide range of nuclei. In addition, in order to further analyze the shell model results concerning the higher-spin structure of yrast states, we also present calculations for these nuclei using the pair-truncated shell model (PTSM) [10–17].

This paper is organized as follows. Section II outlines the general framework of the shell model calculations using the pairing plus quadrupole-quadrupole interactions. The results of the energy levels and electromagnetic transitions are presented in Sec. III. Section IV discusses the structure of high-spin states in terms of the PTSM. Finally the summary and conclusions are given in Sec. V.

II. SHELL MODEL FRAMEWORK

Fully shell-model calculations have been performed for Se, As, Ge, and Ga isotopes assuming a valence space consisting of neutrons and protons occupying $g_{9/2}$, $p_{1/2}$, $p_{3/2}$, and $f_{5/2}$ orbitals. The effective shell-model Hamiltonian is given by

$$H = H_\nu + H_\pi + H_{\nu\pi}, \tag{1}$$

where H_ν, H_π, and $H_{\nu\pi}$ represent the neutron, proton and neutron-proton interactions, respectively. The interaction among like nucleons, H_τ (where $\tau = \nu$ or π), consists of spherical single-particle energies, monopole-pairing (MP) interactions, quadrupole-pairing (QP) interactions, and quadrupole-quadrupole (QQ) interactions

$$H_\tau = \sum_{jm} \varepsilon_{j\tau} c^\dagger_{jm\tau} c_{jm\tau} - G_{0\tau} P^{\dagger(0)}_\tau P^{(0)}_\tau - G_{2\tau} P^{\dagger(2)}_\tau \tilde{P}^{(2)}_\tau - \kappa_\tau : Q_\tau \cdot Q_\tau :, \tag{2}$$

where :: represents the normal ordering. Here $c^\dagger_{jm\tau}$ and $c_{jm\tau}$ are the nucleon creation and the annihilation operators, respectively, and (j, m) represents the quantum numbers necessary to specify a single-particle state. The monopole pair-creation operator $P^{\dagger(0)}_\tau$, the quadrupole pair-creation operator $P^{\dagger(2)}_{M\tau}$, and

*yoshinaga@phy.saitama-u.ac.jp
†koji.higashiyama@it-chiba.ac.jp
‡p.regan@surrey.ac.uk

the quadrupole operator $Q_{M\tau}$ are defined by

$$P^{\dagger(0)}_{\tau} = \sum_{j} \frac{\sqrt{2j+1}}{2} A^{\dagger(0)}_{0\tau}(jj), \tag{3}$$

$$P^{\dagger(2)}_{M\tau} = \sum_{j_1 j_2} Q_{j_1 j_2} A^{\dagger(2)}_{M\tau}(j_1 j_2), \tag{4}$$

$$\tilde{P}^{(2)}_{M\tau} = (-)^M P^{(2)}_{-M\tau}, \tag{5}$$

$$Q_{M\tau} = \sum_{j_1 j_2} Q_{j_1 j_2} \left[c^{\dagger}_{j_1\tau} \tilde{c}_{j_2\tau}\right]^{(2)}_{M}, \quad (\tilde{c}_{jm\tau} = (-1)^{j-m} c_{j-m\tau}), \tag{6}$$

$$Q_{j_1 j_2} = -\frac{\langle j_1 \| r^2 Y^{(2)} \| j_2 \rangle}{\sqrt{5}}, \tag{7}$$

where the creation operator of a pair of nucleons in the orbitals j_1 and j_2 with total angular momentum J and magnetic quantum number M is constructed by

$$A^{\dagger(J)}_{M\tau}(j_1 j_2) = \left[c^{\dagger}_{j_1\tau} c^{\dagger}_{j_2\tau}\right]^{(J)}_{M}. \tag{8}$$

The interaction between neutrons and protons $H_{\nu\pi}$ is taken as

$$H_{\nu\pi} = -\kappa_{\nu\pi} Q_{\nu} \cdot Q_{\pi}. \tag{9}$$

Here the operator Q_τ is the quadrupole operator defined by Eq. (6). Harmonic oscillator basis states with the oscillator parameter $b = \sqrt{\hbar/M\omega}$ are used as the single-particle basis states. The detailed framework of the model is reported in Ref. [18].

III. NUMERICAL RESULTS

A. Energy spectra for even-even isotopes

In the current work the valence neutrons (protons) are treated as holes (particles) relative to the traditional magic numbers at 28 and 50. The adopted single-particle energies for protons and single-hole energies for neutrons are listed in Table I.

The single-particle energies are determined as follows: Since the small difference of single particle energies hardly influences the energy spectra of even-even nuclei, they are determined primarily to reproduce the energy spectra of low-lying states of odd-mass nuclei. First, as the initial guess, they are given from the energy levels of the odd-mass nuclei near the $N = 50$ and $Z = 40$ shell closures. Second, the force strengths of two-body interactions are determined to reproduce the energy spectra of even-even nuclei. Finally, the single particle energies are again modified to give an improved fitting, to the low-energy levels of odd-mass nuclei. The single particle energies are thus obtained by repeating the above procedure several times, iteratively.

TABLE I. Adopted single-particle energies for protons and single-hole energies for neutrons (in MeV).

j	$g_{9/2}$	$p_{1/2}$	$p_{3/2}$	$f_{5/2}$
ε_ν	0.0	0.5	1.0	3.0
ε_π	3.3	1.1	0.6	0.0

Two-body effective interactions are determined as follows: Since the energy spacings between the positive parity states for odd-mass nuclei depend largely on the quadrupole-quadrupole interactions among like nucleons, these interaction strengths are adjusted to fit the experimental energies between the ground states and first excited states with positive parity for odd-mass nuclei. The strengths of the other two-body interactions are determined so as to reproduce the energy levels of the yrast and other low-lying states of even-even nuclei in this mass region.

In order to investigate the energy spectra systematics in this region, we have assumed that the strengths of the effective interactions change linearly with the number of valence neutron holes and proton particles. The adopted strengths of the interactions are as follows: G_0 of MP interaction in units of MeV; G_2 of QP interaction and κ of QQ interaction both in units of MeV/b^4:

$$\begin{aligned}
G_{0\nu} &= 0.16 + 0.03\bar{N}_\nu, \\
G_{2\nu} &= 0.042 + 0.008\bar{N}_\nu, \\
\kappa_\nu &= 0.31 - 0.01\bar{N}_\nu - 0.015N_\pi, \\
G_{0\pi} &= 0.30 - 0.01\bar{N}_\nu - 0.01N_\pi, \\
G_{2\pi} &= 0.06 - 0.002\bar{N}_\nu - 0.006N_\pi, \\
\kappa_\pi &= 0.08 + 0.015\bar{N}_\nu - 0.005N_\pi, \\
\kappa_{\nu\pi} &= -0.20.
\end{aligned} \tag{10}$$

Here $\bar{N}_\nu$ represents the number of neutron holes and N_π the number of proton particles.

Figure 1 shows the theoretical spectra of low-lying positive parity states in ^{84}Se$_{50}$ (i.e., the single-closed nucleus) and ^{82}Se compared to the experimental data for these nuclei. The energies of the yrast 2^+_1, 4^+_1, and 6^+_1 states are well reproduced. The yrare 0^+_2 state appears lower (higher) in energy compared to experiment for ^{84}Se (^{82}Se). The predicted energy gap between the 6^+_1 and 8^+_1 states is smaller than the experimental value in ^{82}Se, but the larger energy gap between the 8^+_1 and 10^+_1 states is qualitatively reproduced.

Figure 2 presents the predicted low-lying positive parity states in ^{78,80}Se and compares them with the experimental data on these nuclei. [Note that of all the nuclei considered in the present work the 6^+ states in ^{78}Se have the largest number of possible shell-model configurations (7,391,183).] The yrast 2^+_1, 4^+_1, and 6^+_1 states are reproduced in addition to the 3^+_1 states. The predicted 0^+_2 state lies lower in energy compared to experiment for ^{78}Se.

Figures 3 and 4 show the theoretical spectra for ^{82}Ge$_{50}$ and ^{76,78,80}Ge compared to the experimental data on these nuclei. By contrast to the result of the Se isotopes, the 0^+_2 states are notably reproduced higher in energy compared to the 2^+_2 states.

Figures 5 and 6 show the theoretical moments of inertia in comparison with the experimental data. It is seen from the figures that the structural change occurs from ^{80}Se to ^{78}Se and from ^{78}Ge to ^{76}Ge.

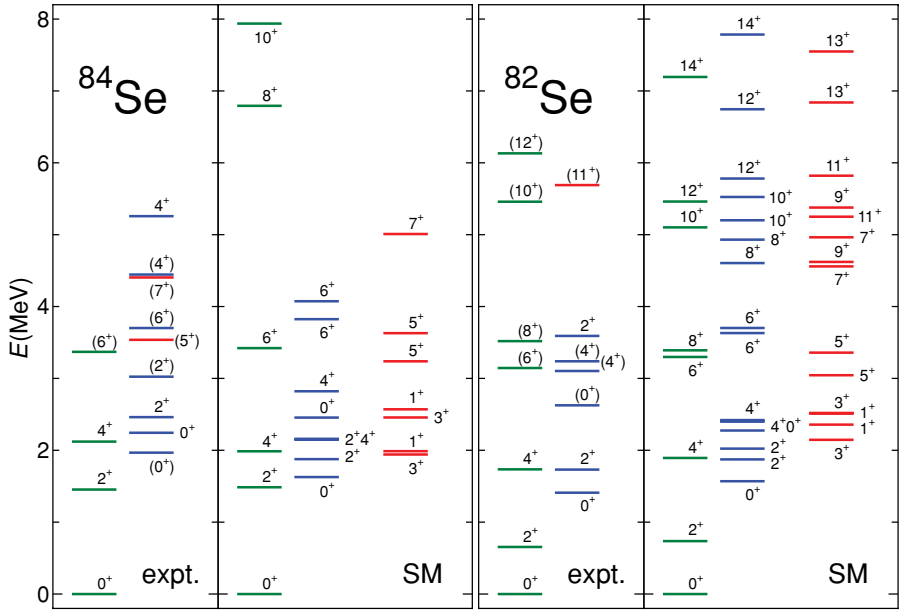

FIG. 1. (Color online) Comparison between the experimental spectra (expt.) and shell model results (SM) for positive parity states in ^{82,84}Se. The experimental data are taken from Refs. [19–21].

B. Negative-parity states

In the simplest excitations for the even-even nuclei of interest in the current work, negative-parity states are produced by either exciting the proton or neutron from a negative-parity orbital into a $g_{9/2}$ orbital. In the shell model these proton and neutron excitations are clearly distinguished. The experimentally reported negative-parity states in Se isotopes (where available) are compared with the shell model calculations in Fig. 7, while the negative parity states in the Ge isotopic chain are shown in Fig. 8. The sparse nature of the experimentally reported negative parity states is in line with the theoretical prediction for the $N = 50$ magic nuclei ^{82}Ge and ^{84}Se, in which no negative-parity states are predicted to lie below an excitation energy of 4 MeV (with the exception of the unconfirmed 1^- state in ^{84}Se).

C. $E2$ transitions

For the $E2$ transition operator we use

$$T(E2;\mu) = e_\nu Q_{\nu\mu} + e_\pi Q_{\pi\mu}, \tag{11}$$

where the effective charges are fixed as $e_\nu = -0.65\,e$ and $e_\pi = 1.65\,e$ using the prescription $e_\pi = (1+\delta)\,e$ and $e_\nu = -\delta\,e$. The value of δ was determined to fit the measured $B(E2; 2_1^+ \rightarrow 0_1^+)$ value in ^{82}Se.

Figure 9 and Table II show the comparison of calculated $B(E2; I \rightarrow I-2)$ values for the yrast states of the selenium isotopes with the experimental data. The shell model calculations predict that the $B(E2)$ values for the positive-parity yrast states reduce around spin $I = 8$ for ^{80,82}Se and $I = 14$ for ^{78}Se compared to the higher spins in these nuclei. In ^{82}Se

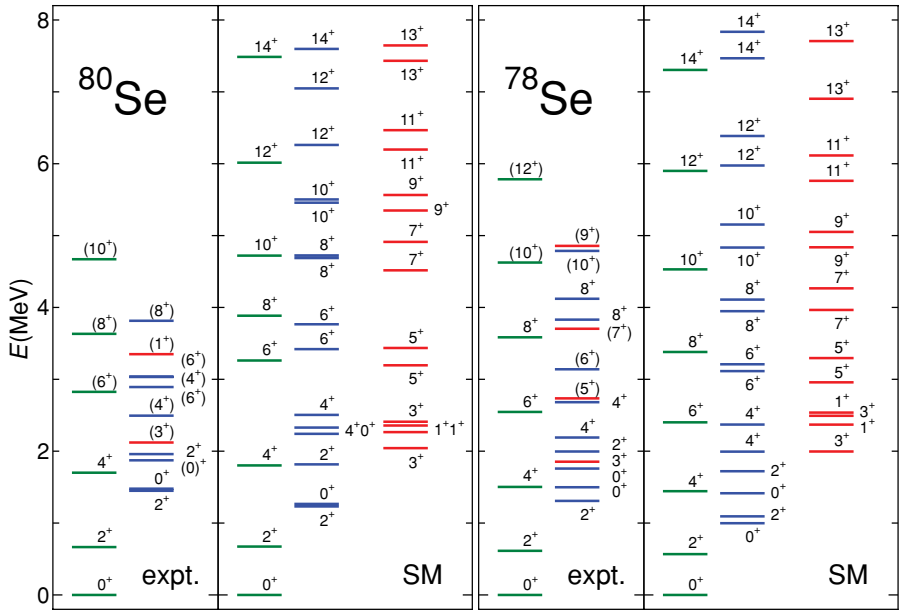

FIG. 2. (Color online) Same figure as in Fig. 1, but for ^{78,80}Se. Experimental data are taken from Refs. [22–24].

TABLE II. Comparison of the calculated $B(E2; I \to I-2)$ values $[B(E2)_{\rm SM}]$ for the yrast states of ^{78,80,82}Se isotopes with experimental data $[B(E2)_{\rm expt.}]$ in Weisskopf units (W.u.). The E_γ values indicate the theoretical γ-ray energies connecting the initial and final states.

I^π	^{82}Se			^{80}Se			^{78}Se		
	E_γ	$B(E2)_{\rm SM}$	$B(E2)_{\rm expt.}$	E_γ	$B(E2)_{\rm SM}$	$B(E2)_{\rm expt.}$	E_γ	$B(E2)_{\rm SM}$	$B(E2)_{\rm expt.}$
2^+	0.736	16.8	16.7 ± 0.3[a]	0.673	23.9	24.2 ± 0.4[a]	0.568	29.0	32.8 ± 4.5[b]
4^+	1.157	23.9	18.7 ± 3.0[a]	1.129	32.4	34.7 ± 1.1[a]	0.876	40.8	$38.2^{+5.6}_{-5.1}$[b]
6^+	1.406	19.5		1.460	32.3		0.958	43.9	48 ± 14[c]
8^+	0.093	0.1	0.56 ± 0.03[d]	0.623	2.6		0.979	47.1	57 ± 19[c]
10^+	1.710	2.1		0.836	21.8		1.149	51.5	
12^+	0.360	2.7		1.293	23.1		1.370	44.2	
14^+	1.734	11.6		1.472	16.5		1.405	23.0	

[a]Taken from Ref. [27].
[b]Taken from Ref. [23].
[c]Taken from Ref. [26].
[d]Taken from Ref. [28].

the experimental $B(E2)$ value drops at spin $I = 8$, which is in accord with the theoretical prediction, while in ^{78}Se the experimental $B(E2)$ values below spin $I = 8$ do not seem to decrease, also in accord with the predicted behavior. The reduction of the $E2$ strengths can be related to the alignment of high-j valence nucleons at these corresponding spins, as discussed later. These two spin values ($I = 8$ and 14) correspond to the alignment of two $g_{9/2}$ neutrons and protons, respectively. In ^{80}Ge, the experimental $B(E2)$ value drops at spin $I = 8$, which is in line with the theoretical prediction.

Figure 10 and Table III show the comparison for the germanium isotopes. Here, the shell model calculations predict that the $B(E2)$ values also drop around spin $I = 8$ for ^{78,80}Ge, but continue with a more constant value with increasing spin in the case of ^{76}Ge.

D. Energy spectra for odd-mass nuclei

Odd-mass nuclei provide an ideal testing ground for predictions of theoretical single particle energies. Using the same set of interactions which was used for even-even nuclei, we have preformed shell-model calculations for odd-mass nuclei in this region.

Figure 11 shows the theoretical spectra for ^{79,81,83}Se and compares them with the experimental data on these nuclei. The experimentally determined spins and parities of the ground states for each of these nuclei are reproduced by the calculations, providing confirmation that the theoretical treatment of the single-particle energies is robust in the current work.

Figures 12, 13, and 14 show the theoretical spectra of ^{77,79,81}As, ^{77,79,81}Ge, and ^{75,77,79}Ga respectively compared with the experimental data. In general, there is good correspondence between the theoretical and experimental levels, with some notable exceptions (for example, in ^{77}Ge where the theoretical negative-parity states appear to all lie systematically higher in energy compared to experiment).

In our present formalism we have not introduced the monopole interaction. Considering the fact that the calculated energy levels in the low-lying states lie much higher than the experimentally observed data, the monopole interaction may need to be introduced to account for these differences in future work.

TABLE III. Same as Table II but for ^{76,78,80}Ge isotopes.

I^π	^{80}Ge			^{78}Ge			^{76}Ge		
	E_γ	$B(E2)_{\rm SM}$	$B(E2)_{\rm expt.}$	E_γ	$B(E2)_{\rm SM}$	$B(E2)_{\rm expt.}$	E_γ	$B(E2)_{\rm SM}$	$B(E2)_{\rm expt.}$
2^+	0.805	14.7	13.6 ± 2.6[a]	0.663	21.4	22.4 ± 1.4[a]	0.569	23.0	29.1 ± 0.3[b]
4^+	1.156	18.5		1.074	28.6		0.897	31.4	38.2 ± 6.8[b]
6^+	1.321	17.9		1.412	31.8		1.020	33.6	
8^+	0.255	0.1	<3[c]	0.891	1.4		1.065	33.7	
10^+	1.301	5.3		0.864	12.9		1.255	36.0	
12^+	1.091	0.2		1.649	11.9		1.573	37.0	
14^+	2.123	0.2		1.866	0.8		1.947	34.5	

[a]Taken from Ref. [30].
[b]Taken from Ref. [29].
[c]Taken from Ref. [28].

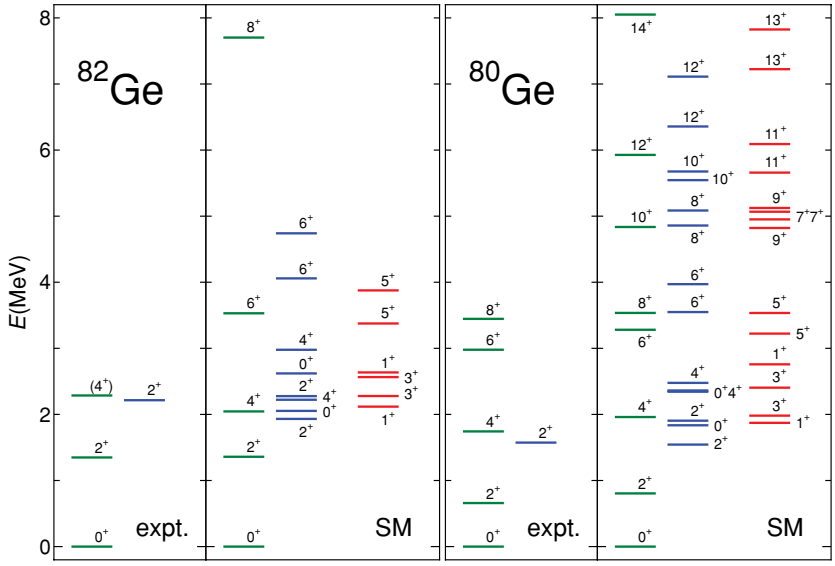

FIG. 3. (Color online) Same figure as in Fig. 1, but for ^{80,82}Ge. Experimental data are taken from Refs. [19,24].

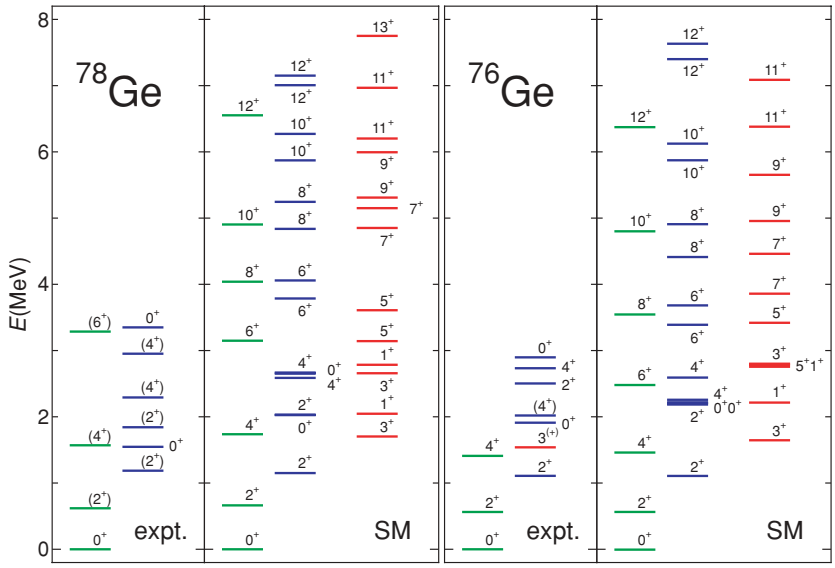

FIG. 4. (Color online) Same figure as in Fig. 1, but for ^{76,78}Ge. Experimental data are taken from Refs. [22,25].

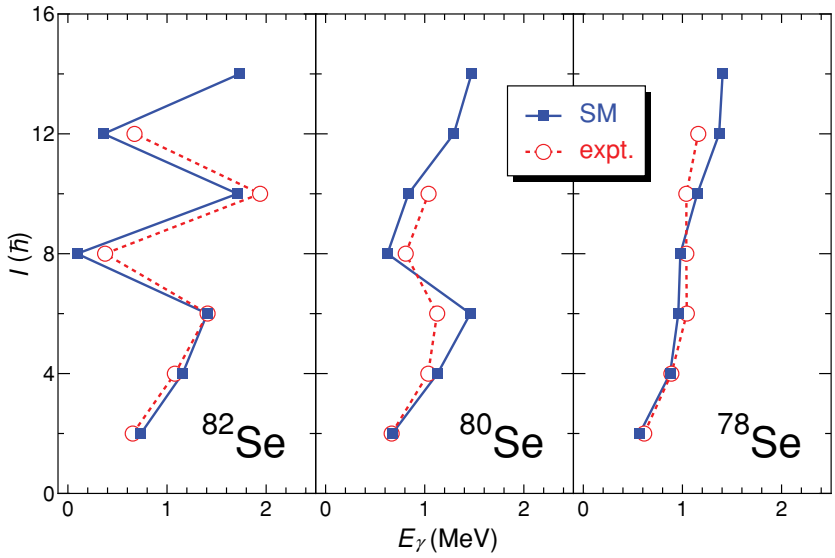

FIG. 5. (Color online) Comparison between experimental moment of inertia (expt.) and shell model results (SM) for Se isotopes.

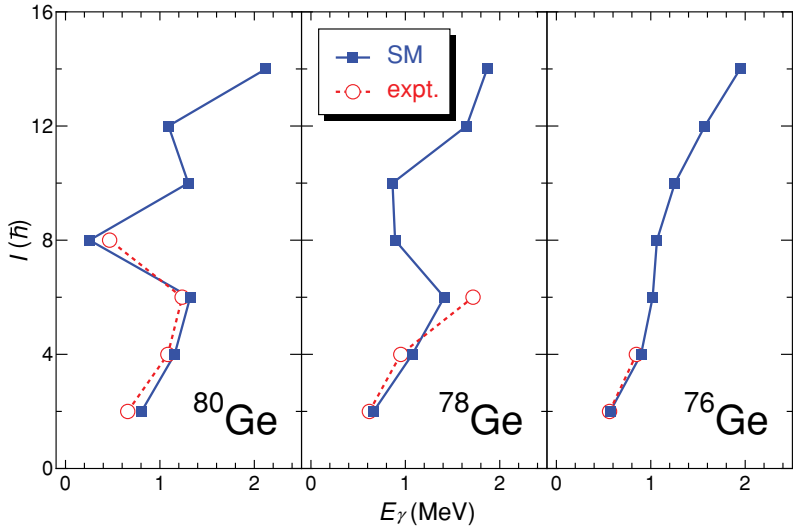

FIG. 6. (Color online) Comparison between experimental moment of inertia (expt.) and shell model results (SM) for Ge isotopes.

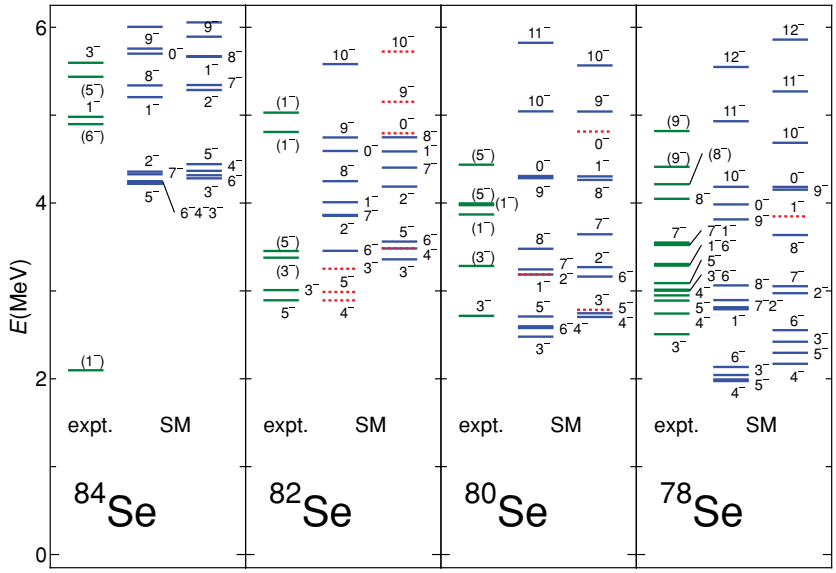

FIG. 7. (Color online) Comparison between experimental spectra (expt.) and shell model results (SM) for negative parity states in the ^{78,80,82,84}Se. Negative parity states arising from the proton valence space are denoted by solid lines while those from the neutron space are shown as dotted lines. The experimental data are taken from Refs. [19,20,22,24].

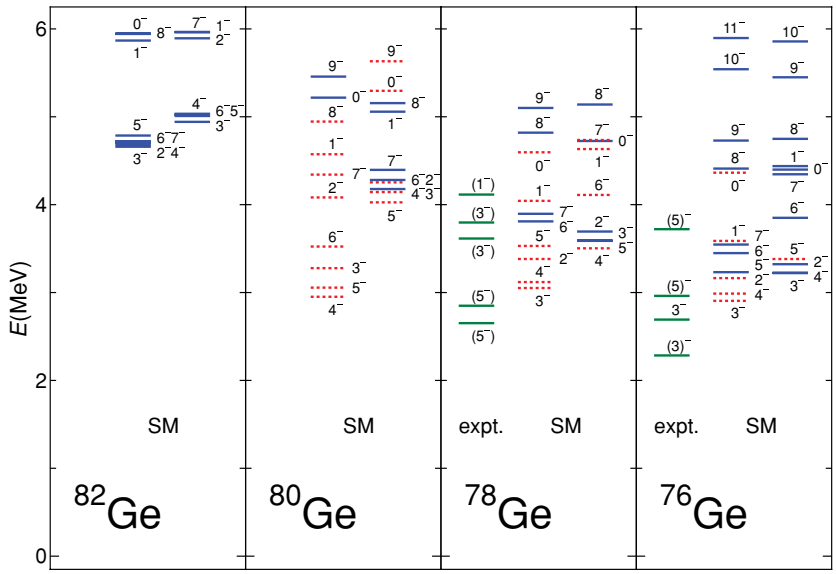

FIG. 8. (Color online) The same for ^{76,78,80,82}Ge as in Fig. 7. The experimental data are taken from Refs. [19,22,24,25].

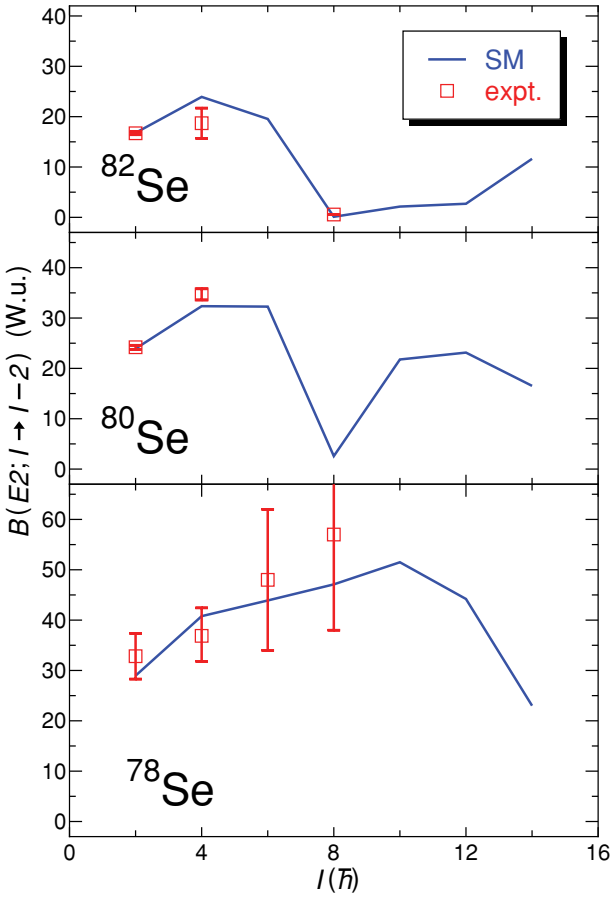

FIG. 9. (Color online) Comparison of the calculated $B(E2)$ values (solid lines) for the yrast states of ^{78,80,82}Se isotopes with experimental data (open squares) taken from Refs. [23,26–28].

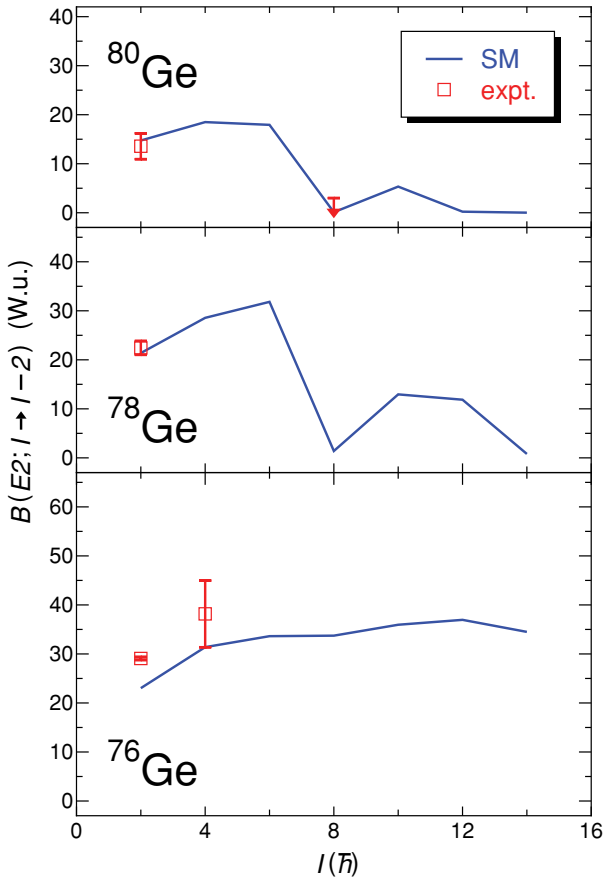

FIG. 10. (Color online) Comparison of the calculated $B(E2)$ values (solid lines) for the yrast states of ^{76,78,80}Ge. The experimental data are taken from Refs. [28–30].

IV. ANALYSIS IN TERMS OF PTSM

In order to investigate the structure of low-lying and higher-spin states, we have also carried out PTSM calculations [10–17] in these nuclei. In the PTSM, low-spin collective pairs are introduced as basic components of the model. Using the pair creation operators $A_M^{\dagger(J)}$ as defined in Eq. (8), we can create angular momenta zero (S), two (D), and four (G) collective pairs:

$$S^\dagger = \sum_j \alpha_j A_0^{\dagger(0)}(jj), \tag{12}$$

$$D_M^\dagger = \sum_{j_1 j_2} \beta_{j_1 j_2} A_M^{\dagger(2)}(j_1 j_2), \tag{13}$$

$$G_M^\dagger = \sum_{j_1 j_2} \gamma_{j_1 j_2} A_M^{\dagger(4)}(j_1 j_2), \tag{14}$$

where the structure coefficients α, β, and γ are determined by variation.

The pair creation operator for the "high angular momentum pair" (H-pair) is defined as

$$H_M^{\dagger(K)} = [c_{9/2}^\dagger c_{9/2}^\dagger]_M^{(K)}, \tag{15}$$

where $K = 0, 2, 4, 6$, and 8. In contrast to the S, D, and G pairs, the H pair is noncollective, since it has a unique structure consisting of the $g_{9/2}$ orbitals.

Using the S, D, G, and H pair-creation operators, a many-body wave function of like nucleons can be constructed by applying creation operators on the closed-shell core $|-\rangle$ as

$$\left|\Psi_{n_s,n_d,n_g,n_h}(I\eta)\right\rangle = (S^\dagger)^{n_s}(D^\dagger)^{n_d}(G^\dagger)^{n_g}(H^\dagger)^{n_h}|-\rangle, \tag{16}$$

where I is a total angular momentum of the many-body state and η, an additional quantum number required to completely specify the state. Here, the number of valence nucleon pairs, $n_s + n_d + n_g + n_h$, is fixed to a constant value for a specific nucleus. The angular momentum coupling is carried out exactly, but we abbreviate its notation. Thus the many-body wave function of the even-even nucleus can be written as

$$|\Phi(I\eta)\rangle = \left[\left|\Psi_{\bar{n}_s,\bar{n}_d,\bar{n}_g,\bar{n}_h}(I_\nu\eta_\nu)\right\rangle \otimes \left|\Psi_{n_s,n_d,n_g,n_h}(I_\pi\eta_\pi)\right\rangle\right]^{(I)}, \tag{17}$$

where $\bar{n}_s, \bar{n}_d, \bar{n}_g$, and $\bar{n}_h$ represent the numbers of neutron-hole S, D, G, and H pairs, respectively, while n_s, n_d, n_g, and n_h correspond to those for proton particle pairs. The $2(\bar{n}_s + \bar{n}_d + \bar{n}_g + \bar{n}_h)$ $(=\bar{N}_\nu)$ and $2(n_s + n_d + n_g + n_h)$ $(=N_\pi)$ are the total numbers of valence neutron-holes and proton-particles, respectively.

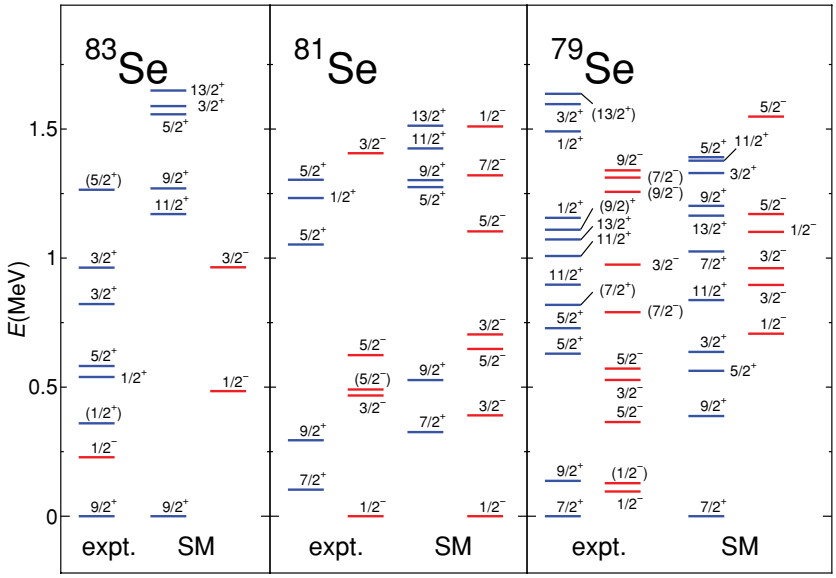

FIG. 11. (Color online) Comparison between the experimental spectra (expt.) and shell model results (SM) for ^{79,81,83}Se. The experimental data are taken from Refs. [31–33].

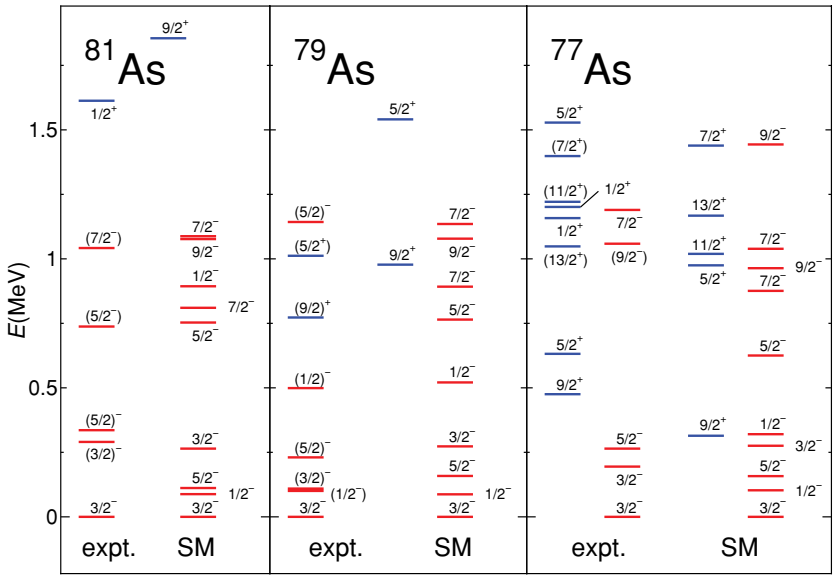

FIG. 12. (Color online) Comparison between the experimental spectra (expt.) and shell model results (SM) for ^{77,79,81}As. The experimental data are taken from Refs. [31,33,34].

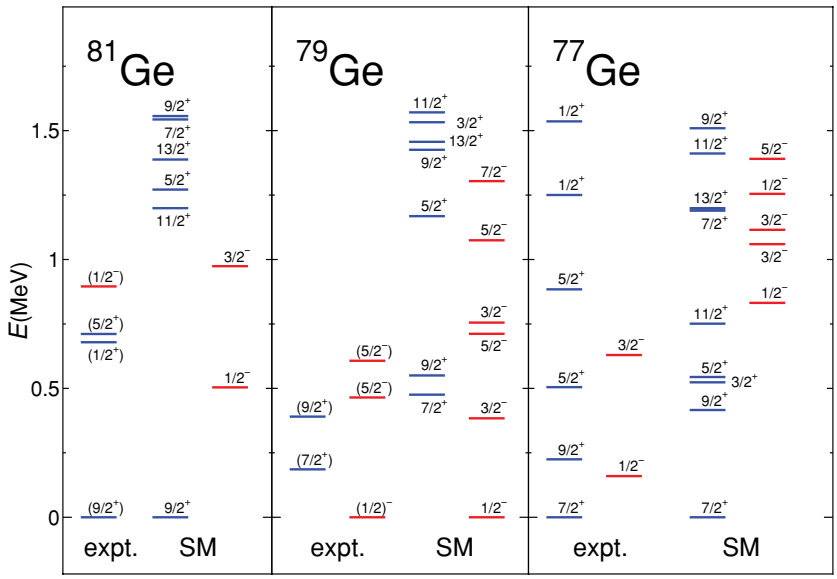

FIG. 13. (Color online) Comparison between the experimental spectra (expt.) and shell model results (SM) for ^{77,79,81}Ge as in Fig. 11. The experimental data are taken from Refs. [31,33,34].

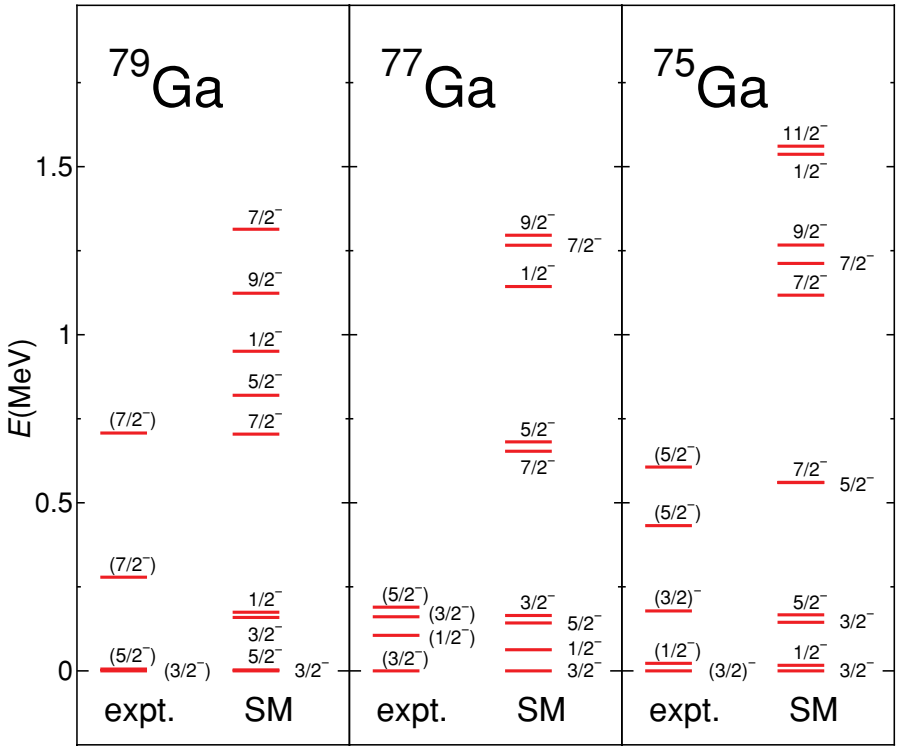

FIG. 14. (Color online) Comparison between the experimental spectra (expt.) and shell model results (SM) for ^{75,77,79}Ga as in Fig. 11. The experimental data are taken from Refs. [33–35].

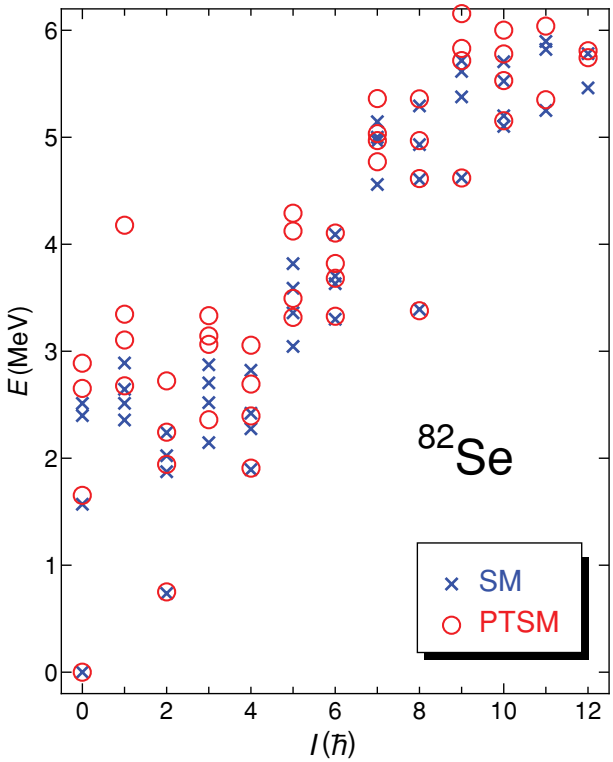

FIG. 15. (Color online) Comparison of the calculated energy levels in the PTSM (open circles) and the shell model results (crosses) for ^{82}Se.

The same interaction as used for the shell model calculations is used for the PTSM calculation. Figure 15 shows the PTSM spectrum for ^{82}Se and compares the PTSM results with those of the full shell model described above. It is evident from the figure that the model space spanned by the PTSM is adequate enough to reproduce the shell model results. In particular, the even-spin yrast states in the shell model are very well reproduced by the PTSM.

In Figs. 16, 17, and 18 the expectation numbers of pairs in the PTSM wave functions for selenium and germanium isotopes are shown as a function of spin I. Figure 16 shows the expectation numbers in ^{82}Se and ^{80}Ge ($N = 48$). For the low-lying states ($I \leqslant 6$), the valence proton excitation is important. It is seen from the figure that the alignment of two $g_{9/2}$ neutrons occurs at spin $I = 8$, while that of two $g_{9/2}$ protons occurs at spin $I = 16$ for both nuclei. Figure 17 shows the expectation numbers for ^{80}Se and ^{78}Ge ($N = 46$). The D_ν and D_π collective pairs are dominant in low-lying states ($I \leqslant 6$), while the effect of the alignment of two $g_{9/2}$ neutrons becomes apparent above spin $I = 8$. The proton alignment does not occur below spin $I = 16$. Figure 18 shows the expectation numbers for ^{78}Se and ^{76}Ge ($N = 44$). In both of these nuclei the numbers of the D_ν collective pairs rapidly increase compared to that of the D_π pairs, indicating that the valence neutron excitation is responsible for the low-lying states. In contrast to the cases for $N = 48$ and 46 isotones, the expectation numbers of the H_ν pairs ($K = 8$) increase slowly around spin $I = 8$. Due to the smooth increases of the expectation numbers of the H_ν pairs ($K = 8$), the

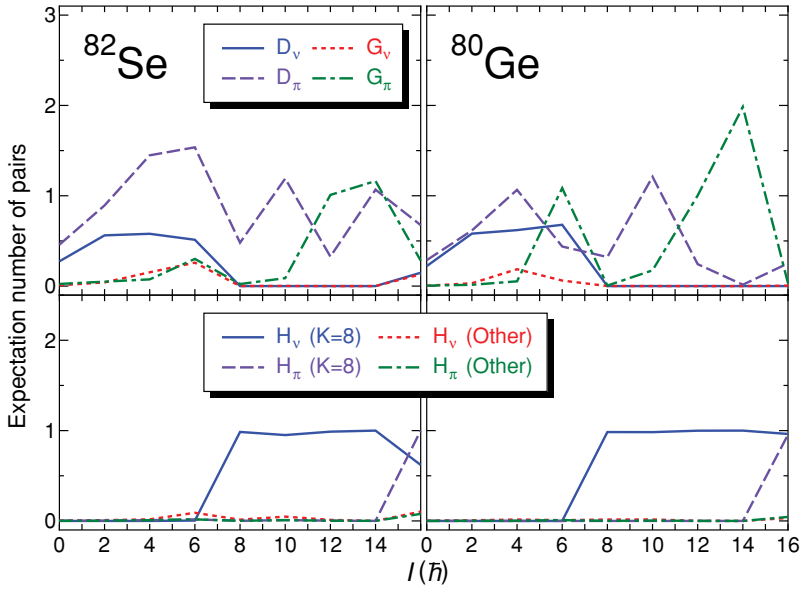

FIG. 16. (Color online) Upper panel: The expectation numbers of D and G pairs calculated in the PTSM for ^{82}Se and ^{80}Ge as a function of spin, I. The solid, dotted, dashed, and dash-dotted lines are for the neutron D pairs, the neutron G pairs, the proton D pairs, and the proton G pairs, respectively. Lower panel: The expectation numbers of H pairs. The solid, dotted, dashed, and dash-dotted lines are the neutron H pairs with angular momentum $K = 8$, the sum of the other neutron H pairs ($K = 0, 2, 4, 6$), the proton H pairs with angular momentum $K = 8$, the sum of the other proton H pairs ($K = 0, 2, 4, 6$), respectively.

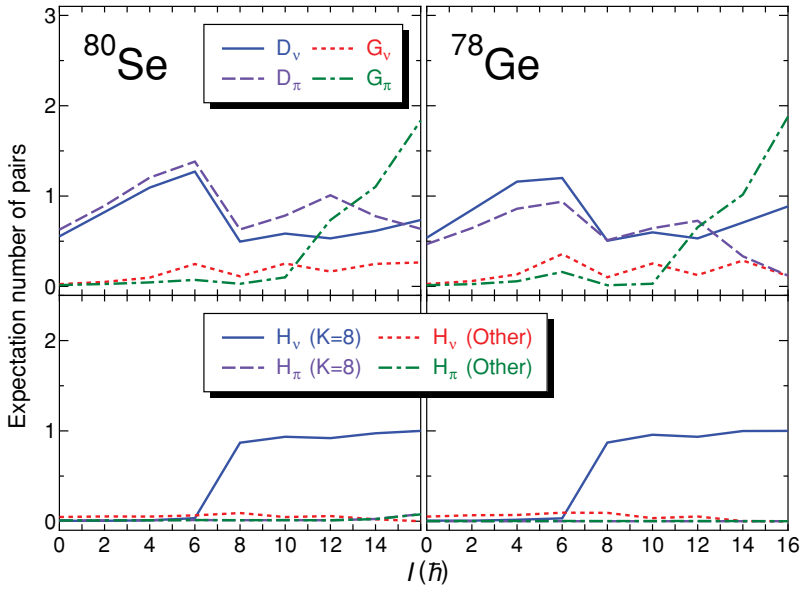

FIG. 17. (Color online) Same figure as in Fig. 16, but for ^{80}Se and ^{78}Ge.

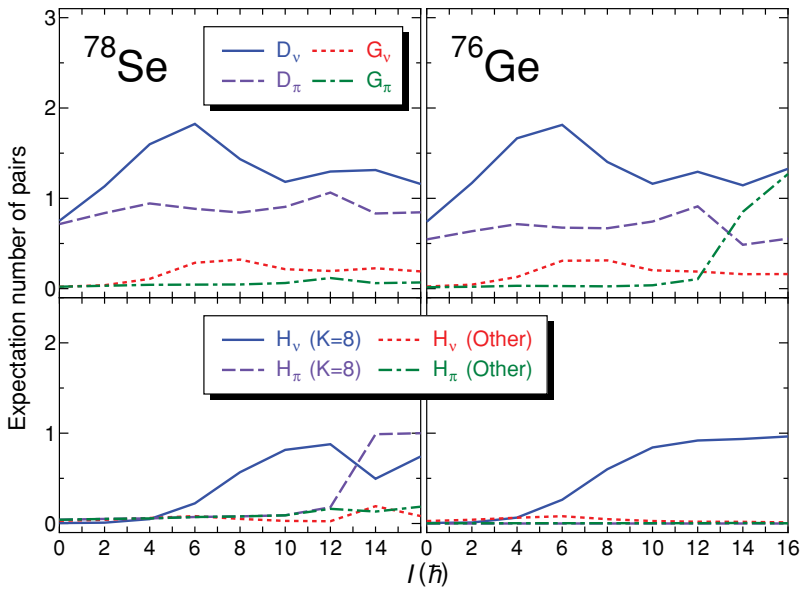

FIG. 18. (Color online) Same figure as in Fig. 16, but for ^{78}Se and ^{76}Ge.

$B(E2)$ values become rather smooth and flat as a function of spin I.

V. SUMMARY AND CONCLUSIONS

In this paper we have investigated the internal structure of the low-lying and near-yrast states in neutron rich even-even and odd-mass Se, As, Ge, and Ga isotopes approaching the $N = 50$ shell closure in terms of the both the full shell model and the PTSM.

In the shell model calculations we have used the pairing plus quadrupole-quadrupole interaction whose strengths vary linearly as functions of valence neutrons and protons. The energy levels of both positive and negative parity states in these isotopes are well reproduced using these simple effective interactions. The calculated $B(E2)$ values obtained give reasonable agreement with experimental data.

The PTSM calculations have also been performed to further interpret the shell model results and are found to provide results consistent with each other. Through the analysis of PTSM wave functions we predict that the structural change evident at ^{80}Se compared to its neighbor ^{78}Se is due to a maximum angular momentum alignment of a pair of neutrons at spin $8\hbar$. A similar effect is also predicted in the Ge isotopes.

ACKNOWLEDGMENTS

The numerical calculations financially supported by Saitama University were carried out partly by the HITACHI SR11000 supercomputers at Supercomputing Division, Information Technology Center, University of Tokyo. The work was supported by Grant-in-Aid for Scientific Research (19740146) and (20540250) from the Ministry of Education, Culture, Sports, Science, and Technology of Japan and the EPSRC/STFC (UK).

[1] S. N. Liddick, P. F. Mantica, R. Broda, B. A. Brown, M. P. Carpenter, A. D. Davies, B. Fornal, T. Glasmacher, D. E. Groh, M. Honma, M. Horoi, R. V. F. Janssens, T. Mizusaki, D. J. Morrissey, A. C. Morton, W. F. Mueller, T. Otsuka, J. Pavan, H. Schatz, A. Stolz, S. L. Tabor, B. E. Tomlin, and M. Wiedeking, Phys. Rev. C **70**, 064303 (2004).

[2] A. Bürger, T. R. Saito, H. Grawe, H. Hübel, P. Reiter, J. Gerl, M. Górska, H. J. Wollersheim, A. Al-Khatib, A. Banu, T. Beck, F. Becker, P. Bednarczyk, G. Benzoni, A. Bracco, S. Brambilla, P. Bringel, F. Camera, E. Clément, P. Doornenbal, H. Geissel, A. Görgen, J. Grębosz, G. Hammond, M. Hellström, M. Honma, M. Kavatsyuk, O. Kavatsyuk, M. Kmiecik, I. Kojouharov, W. Korten, N. Kurz, R. Lozeva, A. Maj, S. Mandal, B. Million, S. Muralithar, A. Neußer, F. Nowacki, T. Otsuka, Zs. Podolyák, N. Saito, A. K. Singh, H. Weick, C. Wheldon, O. Wieland, and M. Winkler (RISING Collaboration), Phys. Lett. **B622**, 29 (2005).

[3] D.-C. Dinca, R. V. F. Janssens, A. Gade, D. Bazin, R. Broda, B. A. Brown, C. M. Campbell, M. P. Carpenter, P. Chowdhury, J. M. Cook, A. N. Deacon, B. Fornal, S. J. Freeman, T. Glasmacher, M. Honma, F. G. Kondev, J.-L. Lecouey, S. N. Liddick, P. F. Mantica, W. F. Mueller, H. Olliver, T. Otsuka, J. R. Terry, B. A. Tomlin, and K. Yoneda, Phys. Rev. C **71**, 041302(R) (2005).

[4] R. V. F. Janssens, B. Fornal, P. F. Mantica, B. A. Brown, R. Broda, P. Bhattacharyya, M. P. Carpenter, M. Cinausero, P. J. Daly, A. D. Davies, T. Glasmacher, Z. W. Grabowski, D. E. Groh, M. Honma, F. G. Kondev, W. Królasb, T. Lauritsen, S. N. Liddick, S. Lunardi, N. Marginean, T. Mizusaki, D. J. Morrissey, A. C. Morton, W. F. Mueller, T. Otsuka, T. Pawlat, D. Seweryniak, H. Schatz, A. Stolz, S. L. Tabor, C. A. Ur, G. Viesti, I. Wiedenhöver, and J. Wrzesiński, Phys. Lett. **B546**, 55 (2002).

[5] B. Fornal, S. Zhu, R. V. F. Janssens, M. Honma, R. Broda, P. F. Mantica, B. A. Brown, M. P. Carpenter, P. J. Daly, S. J. Freeman, Z. W. Grabowski, N. J. Hammond, F. G. Kondev, W. Królas, T. Lauritsen, S. N. Liddick, C. J. Lister, E. F. Moore, T. Otsuka, T. Pawłat, D. Seweryniak, B. E. Tomlin, and J. Wrzesiński, Phys. Rev. C **70**, 064304 (2004).

[6] S. N. Liddick, P. F. Mantica, R.V. F. Janssens, R. Broda, B. A. Brown, M. P. Carpenter, B. Fornal, M. Honma, T. Mizusaki, A. C. Morton, W. F. Mueller, T. Otsuka, J. Pavan, A. Stolz, S. L. Tabor, B. E. Tomlin, and M. Wiedeking, Phys. Rev. Lett. **92**, 072502 (2004).

[7] R. Broda, J. Phys. G **32**, R151 (2006).

[8] B. A. Brown, Prog. Part. Nucl. Phys. **47**, 517 (2001).

[9] G. A. Jones, P. H. Regan, Zs. Podolyák, N. Yoshinaga, K. Higashiyama, G. de Angelis, Y. H. Zhang, A. Gadea, C. A. Ur, M. Axiotis, D. Bazzacco, D. Bucurescu, E. Farnea, W. Gelletly, M. Ionescu-Bujor, A. Iordachescu, Th. Kröll, S. D. Langdown, S. Lenzi, S. Lunardi, N. Marginean, T. Martinez, N. H. Medina, R. Menegazzo, D. R. Napoli, B. Quintana, B. Rubio, C. Rusu, R. Schwengner, D. Tonev, J. J. Valiente Dobón, and W. von Oertzen, Phys. Rev. C **76**, 054317 (2007).

[10] N. Yoshinaga, Nucl. Phys. **A503**, 65 (1989).

[11] N. Yoshinaga and D. M. Brink, Nucl. Phys. **A515**, 1 (1990).

[12] N. Yoshinaga, Nucl. Phys. **A570**, 421 (1994).

[13] N. Yoshinaga, T. Mizusaki, A. Arima, and Y. D. Devi, Prog. Theor. Phys. Suppl. **125**, 65 (1996).

[14] N. Yoshinaga, Y. D. Devi, and A. Arima, Phys. Rev. C **62**, 024309 (2000).

[15] K. Higashiyama, N. Yoshinaga, and K. Tanabe, Phys. Rev. C **67**, 044305 (2003).

[16] N. Yoshinaga and K. Higashiyama, Phys. Rev. C **69**, 054309 (2004).

[17] K. Higashiyama, N. Yoshinaga, and K. Tanabe, Phys. Rev. C **72**, 024315 (2005).

[18] K. Higashiyama, N. Yoshinaga, and K. Tanabe, Phys. Rev. C **65**, 054317 (2002).

[19] J. K. Tuli, Nucl. Data Sheets **98**, 209 (2003).

[20] J. K. Tuli, Nucl. Data Sheets **81**, 331 (1997).

[21] A. Prévost, M. G. Porquet, A. Astier, I. Deloncle, F. Azaiez, A. Buta, D. Curien, O. Dorvaux, G. Duchêne, B. J. P. Gall, F. Khalfallah, I. Piqueras, M. Rousseau, M. Meyer, N. Redon, O. Stézowski, Ts. Venkova, R. Lucas, and A. Bogachev, Eur. Phys. J. A **22**, 391 (2004).

[22] S. Rab, Nucl. Data Sheets **63**, 1 (1991).

[23] T. Hayakawa, Y. Toh, M. Oshima, A. Osa, M. Koizumi, Y. Hatsukawa, Y. Utsuno, J. Katakura, M. Matsuda, T. Morikawa, M. Sugawara, H. Kusakari, and T. Czosnyka, Phys. Rev. C **67**, 064310 (2003).

[24] B. Singh, Nucl. Data Sheets **105**, 223 (2005).

[25] B. Singh, Nucl. Data Sheets **74**, 63 (1995).
[26] R. Schwengner, G. Winter, J. Döiring, L. Funke, P. Kemnitz, E. Will, A. E. Sobov, A. D. Efimov, M. F. Kudojarov, I. Kh. Lemberg, A. S. Mishin, A. A. Pasternak, L. A. Rassadin, and I. N. Chugunov, Z. Phys. A **326**, 287 (1987).
[27] K.-H. Speidel, N. Benczer-Koller, G. Kumbartzki, C. Barton, A. Gelberg, J. Holden, G. Jakob, N. Matt, R. H. Mayer, M. Satteson, R. Tanczyn, and L. Weissman, Phys. Rev. C **57**, 2181 (1998).
[28] A. Makishima, M. Asai, T. Ishii, I. Hossain, M. Ogawa, S. Ichikawa, and M. Ishii, Phys. Rev. C **59**, R2331 (1999).
[29] R. Lecomte, M. Irshad, S. Landsberger, G. Kajrys, P. Paradis, and S. Monaro, Phys. Rev. C **22**, 2420 (1980).
[30] E. Padilla-Rodal, A. Galindo-Uribarri, C. Baktash, J. C. Batchelder, J. R. Beene, R. Bijker, B. A. Brown, O. Castanõs, B. Fuentes, J. Gomez del Campo, P. A. Hausladen, Y. Larochelle, A. F. Lisetskiy, P. E. Mueller, D. C. Radford, D. W. Stracener, J. P. Urrego, R. L. Varner, and C.-H. Yu, Phys. Rev. Lett. **94**, 122501 (2005).
[31] C. M. Baglin, Nucl. Data Sheets **79**, 447 (1996).
[32] S. C. Wu, Nucl. Data Sheets **92**, 893 (2001).
[33] B. Singh, Nucl. Data Sheets **96**, 1 (2002).
[34] A. R. Farhan and B. Singh, Nucl. Data Sheets **81**, 417 (1997).
[35] A. R. Farhan and B. Singh, Nucl. Data Sheets **86**, 785 (1999).